

Hydrothermal synthesis of 1D TiO₂ nanostructures for dye sensitized solar cells

I. Tacchini,^a A. Ansón-Casaos,*^a Youhai Yu,^b M.T. Martínez,^a M. Lira-Cantu^b

^a Instituto de Carboquímica (CSIC), Miguel Luesma 4, E-50018 Zaragoza, Spain

^b Centre d'Investigació en Nanociència i Nanotecnologia (CIN2, CSIC-ICN), Campus UAB, Edifici ETSE 2nd Floor, E-08193, Bellaterra (Barcelona), Spain.

e-mail: alanson@icb.csic.es

Abstract

Mono-dimensional titanium oxide nanostructures (multi-walled nanotubes and nanorods) were synthesized by the hydrothermal method and applied to the construction of dye sensitized solar cells (DSCs). First, nanotubes (TiNTs) and nanotubes loaded with titanium oxide nanoparticles (TiNT/NPs) were synthesized with specific surface areas of 253 m²/g and 304 m²/g respectively. After that, thermal treatment of the nanotubes at 500°C resulted in their transformation into the corresponding anatase nanorods (TiNT-Δ and TiNT/NPs-Δ samples). X-ray diffraction and Raman spectroscopy data indicated that titanium oxide in the pristine TiNT and TiNT/NP samples was converted into anatase phase TiO₂ during the heating. Additionally, specific surface areas and water adsorption capacities decreased after the heat treatment due to the sample agglomeration and the collapse of the inner nanotube channels. DSCs were fabricated with the nanotube TiNT and TiNT/NP samples and with the anatase nanorod TiNT-Δ and TiNT/NPs-Δ samples as well. The highest power conversion efficiency of $\eta = 3.12\%$ was obtained for the TiNT sample, despite its lower specific surface compared with the corresponding nanoparticle-loaded sample (TiNT/NP).

Keywords: Titanium oxide, nanotubes, nanoparticles, nanorods, hydrothermal synthesis, dye sensitized solar cells.

1. Introduction

Dye-sensitized solar cells (DSCs) based on nanostructured titanium dioxide are considered a realistic low-cost alternative to conventional solid state devices [1]. Typical strategies to improve the efficiency of DSCs are the development of new dyes and the research on semiconductor materials that optimize the charge separation process. New nanostructured forms of titanium oxide (nanotubes, nanowires, nanorods) have been synthesized in the last years and could be good candidates for DSC fabrication [2-5]. A high specific surface area is an important characteristic of the titanium oxide substrate as it allows the adsorption of a large number of dye molecules. Titanium oxide nanotubes have large surface areas and aspect ratios. In a tube-like configuration, the number of boundaries among titanium oxide nanostructures decreases compared to TiO₂ nanoparticles, improving the electrical contacts and the charge carriers transport [6-9]. TiO₂ nanotubes can be synthesized by template, hydrothermal, or electrochemical methods [2-5, 10]. Alkaline hydrothermal synthesis of titanium oxide nanostructures can be performed in a large scale with a simple equipment, low-cost chemicals, and high yields. Materials with different morphologies and crystalline structures can be prepared depending on the process conditions. Titanium oxide nanotubes are obtained after hydrothermal treatments at around 130°C [2], while solid nanorods can be prepared by treatments at higher temperatures (> 150°C) [11, 12]. Short nanorods or single crystal rhombic particles with an enhanced efficiency in DSCs can be obtained by a two step hydrothermal method [13]. Also, TiO₂ nanorods can be obtained by treating the hydrothermally synthesized nanotubes at temperatures of higher than 500°C in air [14].

The photovoltaic conversion efficiency of DSCs based on TiO₂ 1D nanostructures like nanotubes, is controlled by their dimensions and crystalline structure [15]. In general, DSC efficiencies increase with the crystallization degree and the aspect ratio of the TiO₂ nanotubes [15]. In this paper, we present the hydrothermal synthesis of 1D titanium oxide nanostructures (nanotubes and nanorods) and their utilization in DSCs. Titanium oxide nanotubes (TiNTs) were synthesized following the hydrothermal method reported by Kasuga et al. [16]. A small variation in the synthesis procedure permits the formation of nanotubes decorated with titanium oxide nanoparticles (TiNT/NPs). Titanium oxide nanorods were prepared by thermal treatment of the nanotube samples in an air atmosphere, resulting in the TiNT- Δ and TiNT/NP- Δ nanorod samples. The titanium

oxide nanostructured samples were characterized by several analytical techniques including electron microscopy, surface area measurements, thermogravimetric analysis (TGA), Raman spectroscopy, and X-ray diffraction. Finally, the as-prepared materials were applied as electrodes in Dye sensitized solar cells (DSCs). The photovoltaic properties obtained for the different samples are discussed.

2. Material and methods

2.1. Synthesis of nanostructured titanium oxide

In a typical synthesis of titanium oxide nanotubes (TiNTs), 4 g of commercial anatase powder (Aldrich 248576) were added to 400 mL of 10M NaOH, and the mixture was stirred for 30 min at ambient temperature. Afterwards, it was heated at 135°C for 24 h in a 1 L Teflon-lined autoclave. A treatment time of 24 h was considered to be sufficient for the dissolution of the starting TiO₂ anatase powder [17]. The white product was filtered and washed with 0.1 N HCl and deionized water. Finally, the powder was dried in an oven at 110°C. The process to synthesize nanotubes decorated with titanium oxide nanoparticles (TiNT/NPs) was identical to that for TiNTs, but the reactant amounts changed. 2 g of commercial anatase were mixed with 200 mL of 10M NaOH and the mixture was heated at 135°C inside the 1 L autoclave. The product was filtered, washed, and dried as for the TiNT material. Titanium oxide nanorods were prepared by thermal treatment of the TiNT and TiNT/NP materials in a horizontal quartz reactor under an air flow. The heat treatment was controlled using a furnace constructed by Carbolite, UK. Samples were heated to 500°C at 10°C/min, and kept at that temperature for 1h. The resultant materials are labeled as TiNT-Δ and TiNT/NP-Δ respectively. Before the heat treatment, the starting TiNT and TiNT/NP samples were fully exchanged with Ca²⁺ to try to stabilize the nanostructures and preserve their aspect ratio during the heating [18].

2.2. Characterization of titanium oxide powders

The samples were characterized by scanning electron microscopy (SEM, Hitachi S-3400N), and transmission electron microscopy (TEM, JEOL-200FXII). Energy dispersive X-Ray (EDX) spectroscopy was carried out in the SEM equipment. For TEM sample preparation, the sample was suspended in acetone, bath sonicated for 5 min, and dropped onto a Lacey film. Previously to SEM observation, a 10 nm gold film was sputtered on 10 mg of the sample.

Nitrogen adsorption analysis at -196°C was performed in a Micromeritics ASAP 2020 equipment. Water adsorption isotherms at 25°C were measured in a gravimetric system (VTI Corp.) provided with a magnetic suspension balance (Rubotherm). X-ray photoelectron spectroscopy (XPS) measurements were carried out in a ESCAPlus Omicron system provided with a Mg anode (1253.6 eV) working at 150W . Thermogravimetric analysis (TGA) was carried out in a Setaram balance, model Setsys Evolution. X-ray diffraction (XRD) measurements were performed at room temperature on a Bruker AXS D8 Advance diffractometer using $\text{CuK}\alpha$ radiation. Raman spectra were obtained in a HORIBA Jobin Yvon spectrometer, model HR 800 UV working with a 532 nm laser.

2.3. Assembling and characterization of DSCs

Nanoporous TiO_2 electrodes were prepared on a FTO glass (4 mm thickness, Nippon Sheet Glass, SnO_2 : F, 10 ohm/sq) from a TiNT paste by screen-printing technique as previously reported method [19]. The FTO glass was first cleaned in a detergent solution using an ultrasonic bath for 20 min , and then rinsed with water and ethanol. After cleaning with a UV- O_3 system (PSD-UV, Novascan, IA, USA) for 20 min , the FTO glass plates were immersed into a 40 mM aqueous TiCl_4 solution at 70°C for 30 min and washed with water and ethanol. A layer of paste (made from TiNT powders) was coated on the FTO glass plates by screen-printing, kept in a clean box for 6 min so that the paste can relax to reduce the surface irregularity and then dried for 6 min at 125°C . This screen-printing procedure with paste (coating, storing and drying) was repeated four times for the working electrode. The electrodes coated with the TiNT pastes were gradually heated under an airflow at 275°C for 5 min , at 375°C for 5 min , and at 450°C for 15 min , and finally, at 500°C for 15 min . The resulting TiO_2 films were cut into pieces. After cooling to 80°C , the TiO_2 electrode was immersed into a $5.0 \times 10^{-4}\text{ M}$ N719 dye solution in a mixture of acetonitrile and tertbutyl alcohol (volume ratio, 1:1) and kept at room temperature for $20\text{--}24\text{ h}$ to ensure a complete sensitizer uptake. To prepare the counter electrode, a hole (0.5-mm diameter) was drilled in the FTO glass. The perforated sheet was washed with detergent solution and H_2O and sonicated in ethanol for 20 min . After removing residual organic contaminants by UV- O_3 cleaning, the Pt paste (Solaronix) was deposited on the FTO glass by doctor blade method using 2 layers of 3M tape as the spacer. The dye-covered TiNT electrode and the Pt electrode were assembled into a sandwich type cell and sealed with a thermal adhesive film

(SX1170-25, Solaronix, 25 μm of thickness). The size of the TiNT electrodes was 0.196 cm^2 . The hole in the counter electrode was covered with a thermal adhesive film and sealed using a hot iron bar protected by a fluorine polymer film. A hole in the film was then made using a needle. A drop of electrolyte (AN-50 from Solaronix) was put on the hole in the back of the counter electrode. It was introduced into the cell via vacuum backfilling. The cell was placed in a small vacuum chamber to remove air from inside. Exposing it again to ambient pressure caused the electrolyte to be driven into the cell. Finally, the hole was sealed using a thermal adhesive film and a cover glass (0.1 mm thickness). In order to have a good electrical contact for the connections to the measurement set-up, some solder was applied on each side of the FTO electrodes. The position of the solder was 1 mm away from the edge of the thermal adhesive film gasket and hence 4 mm away from the side of the photoactive TiNT layer. The solar simulation for the analyses of the solar cells was carried out with a Steuernagel Solarkonstant KHS1200 equipped with an AM1.5 filter (1000 W/m^2 , AM1.5G, 72°C). The calibration was made according to ASTM G173. IV-curves were measured using a Keithley 2601 multimeter. Light intensity was 1000 W/m^2 . A Zipp & Konen CM-4 pyranometer was used during the measurements to set light intensity and a calibrated S1227-1010BQ photodiode from Hamamatsu was also applied for calibration before each measurement. Incident photon-to-photocurrent efficiency (IPCE) analyses were carried out with a QE/IPCE measurement system from Oriel at 10 nm intervals between 300 and 700 nm. The results were not corrected for intensity losses due to light absorption and reflection by the glass support.

Desorption of the dye from the TiO_2 electrodes was performed after DSC fabrication and photovoltaic characterization. The two electrodes were separated by applying heat and then the sintered TiO_2 electrode was immersed in 3 mL of a 1 mM KOH solution for 1 hour. After that, the solution presented the typical pink colour and the electrode appeared colourless, indicating the effective desorption of the dye. The dye concentration in the solution was determined by UV-Vis spectroscopy.

3. Results and discussion

Figure 1 shows a representative SEM image of the TiNT sample. The powder material consists of aggregates that have a fibrous texture. Particles of the original anatase powder are not observed, indicating that they were dissolved during the hydrothermal treatment. TEM images (Figure 2) demonstrate that both the TiNT and TiNT/NP

powders contain entangled multi-walled nanotubes with at least four walls. Nanotubes have lengths up to 1-3 μm , outer diameters between 7 and 10 nm, inner diameters of 5 nm, and an inter-wall spacing of approximately 0.5 nm. Nanoparticles of 3-4 nm, as well as a kind of amorphous titanium oxide material, can be observed on the nanotube surfaces only on the TiNT/NP sample (Figure 2 c and d). TiNT- Δ and TiNT/NP- Δ powders contain nanorods that are mostly joined in bundles of 5-10 units (bundle thickness \sim 100-200 nm). Individual nanorods have diameters of \sim 20 nm and lengths up to 1-2 μm . They do not have inner channels (Figure 2.f).

Specific surface areas of titanium oxide powders were calculated from nitrogen adsorption data and are listed in Table 1. For all the samples, nitrogen adsorption isotherms at -196°C are type II with a narrow hysteresis loop at $p/p^0 > 0.7$ (Figure 3). Specific surface areas for TiNT and TiNT/NP powders are of 253 m^2/g and 304 m^2/g respectively. The presence of titanium oxide nanoparticles and amorphous material on the nanotubes could be responsible for the surface area difference between the TiNT and TiNT/NP samples. In both cases, the surface area is much larger than in the original commercial anatase (8 m^2/g) due to the open mesoporous structure of titanium oxide nanotubes. Pore size distributions for the nanotube samples (Figure 4) demonstrate the presence of mesopores of \sim 4 nm, as well as two sets of aggregate pores of \sim 10 and \sim 50 nm. Mesopores of 4 nm could be associated to the inner nanotube channels, while 10 nm pores could correspond to adsorption sites in the entangled nanotube network. Pores of \sim 50 nm could be assigned to big spaces between the nanotube aggregate particles that can be observed in SEM images (Figure 1).

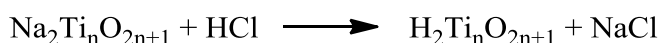
Surface areas of the thermally treated samples (TiNT- Δ and TiNT/NP- Δ) are around 100 m^2/g , which is substantially lower than for the untreated powders. This is indicative of the collapse of the nanotube mesoporous structure during the heating. Mesopores of 4 and 10 nm are greatly reduced (Figure 4) due to the closing of nanotube channels and the aggregation of nanorods into bundles. Also, it was observed that the thermal treatment causes a decrease in the water adsorption capacity of nanotube samples, which is initially much higher than for commercial anatase. Water adsorption capacity of TiNTs at 10 Torr decrease from 10.8 to 8.6 wt% when the powders are dried at 350°C instead of 130°C under vacuum.

The crystalline structure of the samples was studied by Raman spectroscopy (Figure 5) and XRD (Figure 6). Raman spectra of the TiNT and TiNT/NP samples (Figure 5.a and b) show features at \sim 120, 275, 283, 457 and 669 cm^{-1} , which are typically detected in

hydrothermally synthesized titanium oxide nanotubes [20, 21]. The origin of these bands is not completely clear, but is usually associated with Ti-O-Ti crystal phonons in titanate structures [2]. Spectra of TiNT and TiNT/NP samples also show features at $\sim 150, 191, 413$ and 640 cm^{-1} , which correspond to the anatase TiO_2 modes [20, 21], although the intensity of anatase bands in titanium oxide nanotubes is much lower than in crystalline anatase (Figure 5.e). The presence of the anatase bands in nanotube samples could be explained in two ways: 1) the signals are originated by undissolved very small particles of the anatase precursor or 2) anatase bands are actually intrinsic to the titanium oxide nanotube structures. Both explanations would be in agreement with SEM observations and XRD patterns. Raman spectra of the thermally treated samples (TiNT- Δ and TiNT/NP- Δ , Figure 5.c and d) are almost identical to commercial anatase (Figure 5.d). Titanate bands disappear after the treatment at 500°C .

XRD patterns of the TiNT and TiNT/NP samples (Figure 6.a and b) are similar to those reported in the literature for titanium oxide nanotubes [20, 21]. The bands are broad and have low intensity, corresponding to highly polycrystalline materials composed of very small size crystallites. Features at $2\theta \sim 10, 24$ and 48 are commonly assigned to titanate structures such as $\text{H}_2\text{Ti}_n\text{O}_{n+1}$ ($n = 2, 3, 4$) [22-24]. Alternatively, models based on modified anatase structures have been proposed to explain nanotube diffractograms [25]. XRD patterns for the TiNT and TiNT/NP samples could correspond to a mixture of different randomly oriented structures and cannot be directly indexed. Diffractograms of the TiNT- Δ and TiNT/NP- Δ samples (Figure 6.c and d) show the characteristic features of anatase TiO_2 (Figure 6.e) in agreement with Raman spectroscopy results.

Chemical analysis of the titanium oxide samples was performed by means of EDX, XPS and TGA techniques. The results are summarized in Table 1. Sodium was not detected by EDX or XPS in the TiNT and TiNT/NP samples, indicating that all the Na^+ incorporated during the alkaline treatment was eliminated or exchanged by hydrogen during the washing with HCl:



O/Ti atomic ratios of the TiNT and TiNT/NP samples calculated from EDX are higher than 2, suggesting the existence of titanate structures. However, the presence of strongly adsorbed water could alter the amount of oxygen detected by EDX. O/Ti ratios for the TiNT- Δ and TiNT/NP- Δ samples are around 2, as it would be expected for anatase TiO_2 . O/Ti ratios calculated from XPS for all the samples are approximately of 2. No

differences were observed in Ti 2p XPS spectra between the samples before and after the thermal treatment at 500°C, while a slight decrease in the O 1s signal intensity occurred at ~ 531 eV (Figure 7).

TGA profiles of the TiNT and TiNT/NP samples are similar to others previously reported for hydrothermal titanium oxide nanotubes [21, 24]. Weight losses occur in the whole temperature range up to 500°C, but mostly take place at around 100°C. Weight losses at low temperature are due to desorption of moisture or physically adsorbed water. In some previous reports [24], it is assumed that hydrothermal nanotubes have titanate structures ($O/Ti > 2$), and structural water is released during the heating, when the titanate is converted into anatase TiO_2 . In that case, the composition of the titanate structure could be tentatively determined from the TGA weight loss. However, it is not easy to separate the contribution of crystallization water from weight losses caused by strongly physisorbed water.

The characteristics of DSCs built with all the titanium oxide samples are presented in Figure 8 and the detailed photovoltaic values are listed in Table 2. The first observation is that the nanorod samples (TiNT- Δ and TiNT/NP- Δ) show the lowest photovoltaic response. This is contrary to samples treated in a similar way and reported in the literature [14]. Nevertheless, in our work such behavior is in good agreement with the collapse of the TiO_2 nanostructure and the reduction of surface area of the materials after thermal treatment. The highest photovoltaic response was observed for the nanotube sample (TiNT) with a short circuit photocurrent density of 5.87mAcm^{-2} , an open circuit voltage of 711 mV, and a fill factor of 0.645, corresponding to an overall conversion efficiency of 3.12% (Figure 8A.a). The corresponding IPCE spectrum (Figure 8B.a) also shows the highest value, in good agreement with the corresponding I-V curves (Figure 8A). In previous literature reports, some solid mixtures containing both titanium oxide nanotubes and nanoparticles demonstrated improved efficiencies when applied in DSCs. For example, the addition of TiO_2 nanotubes synthesized hydrothermally improved the efficiency of commercial anatase nanoparticles [26, 27]. Also, the efficiency of DSCs containing titania nanotubes synthesized electrochemically increased when the tubes were decorated with TiO_2 nanoparticles [28]. In these cases, the nanoparticles were incorporated to the nanotubes after the nanotube synthesis. However, the best photovoltaic response in our work was observed for the TiO_2 nanotube sample alone (TiNT), and not for the nanotube sample decorated with nanoparticles (TiNT/NP), as one would have expected. The inclusion of nanoparticles

and some amorphous material in the nanotube scaffolding (Figure 2.d) seems to be detrimental for the photocatalytic efficiency. The small increase in the specific surface area of the TiNT/NP sample compared with the TiNT sample do not compensate the loss of the purely nanotubular structure. This effect could be attributed to the structural and electronic properties of the nanotubes, which are decisive in the utilized photovoltaic cell configuration. In fact, femtosecond-nanosecond studies demonstrated that electron injection from the dye to titanium oxide is faster for nanotubes than for nanorods and nanoparticles [29].

Photovoltaic measurements demonstrate that morphology at the nanoscale level is as decisive for DSC efficiency as it is TiO₂ crystal structure and surface area. The important role of 1D nanotubular structures in photovoltaic efficiencies is also supported by the fact that other characteristics of the assembled DSCs were nearly identical for all the tested samples. For example, Figure 9 shows SEM lateral images of the sintered TiO₂ electrodes. The electrodes were porous and had average thicknesses of ~ 1 μm. Surface topography was similar for all the samples.

In order to analyze the dye adsorption capacity of each electrode, we carried out dye-desorption experiments. Desorption of the dye was carried out until its total extraction from the electrode into a KOH solution. Figure 10 shows the UV-Vis spectra of the extract obtained for each sample. All the samples showed similar dye concentrations, in the range of $1.6\text{-}2.4 \cdot 10^{-4}$ mmol/cm² of electrode. When samples with nanotubular morphology (TiNT and TiNT/NP) and samples without tubular morphology (TiNT-Δ and TiNT/NP-Δ) are separately compared, a correlation is observed between the amount of dye adsorbed and the power conversion efficiency of the final device. An increase in the photovoltaic properties would be expected with an increase in the amount of adsorbed dye. However, the TiNT-Δ and TiNT/NP-Δ electrode materials showed slightly higher dye concentrations and lower photovoltaic efficiencies than the TiNP and TiNT-NP materials. This fact could be associated with the 1D tubular nanostructure of the TiNP and TiNT-NP samples.

Conclusions

We synthesized 1D TiO₂ nanostructures and applied them in DSCs. Multi-walled titanium oxide nanotubes (TiNTs) and nanotubes loaded with titanium oxide nanoparticles (TiNT/NPs) were obtained by the hydrothermal method. Controlling the synthesis and post-treatment conditions allows for the modification of the nanostructure

of the materials, which ranged from nanotubes, nanotubes decorated with nanoparticles and nanorods. The crystalline degree of the hydrothermally synthesized materials increases after heat treatment at 500°C (TiNT- Δ and TiNT/NP- Δ), but photovoltaic efficiencies of the respective DSCs are lower than for the untreated materials. The best power conversion efficiency of the solar cells (3.2 %) was obtained for the nanotube sample (TiNT) and not for the nanotubes decorated with nanoparticles (TiNT/NPs), despite the TiNT specific surface area is somewhat lower. The photovoltaic response could be attributed to the structural and electronic properties of the nanotubes, which demonstrate a better performance than the other nanostructures investigated.

Acknowledgements

This work was funded by the Government of Aragon and La Caixa (project ref. GALC-041/2008 and by the Spanish MICINN (projects ref. EUI2008-00152 and ENE2008-04373). We thank the Spanish National Research Council (CSIC) for the JAE-Doc contracts awarded to Y.Y. and A.A. To the Xarxa de Referència en Materials Avançats per a l'Energia, XaRMAE (Reference Center for Advanced Materials for Energy) of the Catalonia Government.

Supplementary Information

Water adsorption isotherms at 25°C. Raman shifts for the band maxima in Figure 5 spectra. TGA analysis.

References

- [1] M. Grätzel, J. Photoch. Photobio. C 4 (2003) 145-153.
- [2] D.V. Bavykin, J.M. Friedrich, F.C. Walsh, Adv. Mater. 18 (2006) 2807-2824.
- [3] S. Uchida, R. Chiba, M. Tomiha, N. Masaki, M. Shirai, Electrochemistry 70 (2002) 418-420.
- [4] G.K. Mor, K. Shankar, M. Paulose, O.K. Varghese, C.A. Grimes, Nano Lett. 6 (2006) 215-218.
- [5] G.K. Mor, O.K. Varghese, M. Paulose, K. Shankar, C.A. Grimes. Solar. Energ. Mater. Sol. Cells 90 (2006) 2011-2075.
- [6] I. Gonzalez-Valls, M. Lira-Cantu, Energy Environ. Sci. 2 (2009) 19-34.
- [7] I. Gonzalez-Valls, M. Lira-Cantu, Energy Environ. Sci. 3 (2010) 789-795.

- [8] L. González-García, J. González-Valls, M. Lira-Cantu, A. Barranco, A.R. González-Elipe, *Energy Environ. Sci.* (2011), doi: 10.1039/C0EE00489H
- [9] S. Ngamsinlapasathian, S. Sakulkaemaruehai, S. Pavasupree, A. Kitiyanan, T. Sreethawong, Y. Suzuki, S. Yoshikawa, *J. Photoch. Photobio. A* 164 (2004) 145-151.
- [10] I. Tacchini, E. Terrado, A. Anson, M.T. Martinez, *J. Mater. Sci.* 46 (2011) 2097-2104.
- [11] Y. Lan, X. Gao, H. Zhu, Z. Zheng, T. Yan, F. Wu, S.P. Ringer, D. Song, *Adv. Funct. Mater.* 15 (2005) 1310-1318.
- [12] J. Jitputti, Y. Suzuki, S. Yoshikawa, *Catal. Commun.* 9 (2008) 1265-1271.
- [13] Y. Xu, X. Fang, Z. Zhang, *Appl. Surf. Sci.* 255 (2009) 8743-8749.
- [14] J. Qu, X.P. Gao, G.R. Li, Q.W. Jiang, T.Y. Yan, *J. Phys. Chem. C* 113 (2009) 3359-3363.
- [15] A. Chicov, S.P. Albu, R. Hahn, D. Kim, T. Stergiopoulos, J. Kunze, C.A. Schiller, P. Falaras, P. Schmuki, *Chem. Asian J.* 4 (2009) 520-525.
- [16] T. Kasuga, M. Hiramatsu, A. Hoson, T. Sekino, K. Nihara, *Adv. Mater.* 11 (1999) 1307-1311.
- [17] D.L. Morgan, G. Triani, M.G. Blackford, N.A. Raftery, R.L. Frost, E.R. Waclawik, *J. Mater. Sci.* 46 (2011) 548-557.
- [18] B.A. Marinkovic, P.M. Jardim, E. Morgado Jr., M.A.S. de Abreu, G.T. Moure, F. Rizzo, *Mater. Res. Bull.* 43 (2008) 1562-1572.
- [19] S. Ito, T.N. Murakami, P. Comte, P. Liska, C. Grätzel, M.K. Nazeeruddin, M. Grätzel, *Thin Solid Films* 516 (2008) 4613-4619.
- [20] A. Gajovic, I. Friscic, M. Plodinec, D. Ivekovic, *J. Mol. Struct.* 924-926 (2009) 183-191.
- [21] S. Mozia, E. Borowiak-Palén, J. Przepiórski, B. Grzmil, T. Tsumura, M. Toyoda, J. Grzechulska-Dumszel, A.W. Morawski, *J. Phys. Chem. Solids* 71 (2010) 263-272.
- [22] A. Nakahira, W. Kato, M. Tamai, T. Isshiki, K. Nishio, H. Aritani, *J. Mater. Sci.* 39 (2004) 4239-4245.
- [23] Q. Chen, W. Zhou, G. Du, L.M. Peng, *Adv. Mater.* 14 (2002) 1208-1211.
- [24] T. Gao, H. Fjelivag, P. Norby, *Inorg. Chem.* 48 (2009) 1423-1432.
- [25] G. Mogilevsky, Q. Chen, A. Kleinhammes, Y. Wu, *Chem. Phys. Lett.* 460 (2008) 517-520.
- [26] D. Wang, B. Yu, F. Zhou, C. Wang, W. Liu, *Mater. Chem. Phys.* 113 (2009) 602-606.

- [27] X.D. Li, D.W. Zhang, S.Chen, Z.A. Wang, Z. Sun, X.J. Yin, S.M. Huang, Mater. Chem. Phys. 124 (2010) 179-183.
- [28] P. Roy, D. Kim, I. Paramasivan, P. Schmuki, Electrochem. Commun. 11 (2009) 1001-1004.
- [29] M. Ziolk, I. Tacchini, M.T. Martinez, X. Yang, L. Sun, A. Douhal, Phys. Chem. Chem. Phys. 13 (2011) 4032-4044.